

# GOING WITH THE FLOW: CAN THE BASE OF JETS SUBSUME THE ROLE OF COMPACT ACCRETION DISK CORONAE?

SERA MARKOFF<sup>1</sup> AND MICHAEL A. NOWAK

Massachusetts Institute of Technology, Kavli Institute for Astrophysics and Space Research, Rm. NE80-6035, Cambridge, MA 02139

AND

JÖRN WILMS

Department of Physics, University of Warwick, Coventry, CV4 7AL, United Kingdom

*Draft version March 28, 2018*

## ABSTRACT

The hard state of X-ray binaries (XRBs) is characterized by a power law spectrum in the X-ray band, and a flat/inverted radio/IR spectrum associated with occasionally imaged compact jets. It has generally been thought that the hard X-rays result from Compton upscattering of thermal accretion disk photons by a hot, coronal plasma whose properties are inferred via spectral fitting. Interestingly, these properties—especially those from certain magnetized corona models—are very similar to the derived plasma conditions at the jet footpoints. Here we explore the question of whether the ‘corona’ and ‘jet base’ are in fact related, starting by testing the strongest premise that they are synonymous. In such models, the radio through the soft X-rays are dominated by synchrotron emission, while the hard X-rays are dominated by inverse Compton at the jet base – with both disk and synchrotron photons acting as seed photons. The conditions at the jet base fix the conditions along the rest of the jet, thus creating a direct link between the X-ray and radio emission. We also add to this model a simple iron line and convolve the spectrum with neutral reflection. After forward-folding the predicted spectra through the detector response functions, we compare the results to simultaneous radio/X-ray data obtained from the hard states of the Galactic XRBs GX 339–4 and Cygnus X-1. Results from simple Compton corona model fits are also presented for comparison. We demonstrate that the jet model fits are statistically as good as the single-component corona model X-ray fits, yet are also able to address the simultaneous radio data.

*Subject headings:* X-rays: binaries—black hole physics—radiation mechanisms: non-thermal—accretion, accretion disks—X-rays: general

## 1. INTRODUCTION

Bipolar plasma outflows, loosely termed jets, are a feature common to a variety of different astrophysical objects. Jets are observed in accreting compact objects of all scales, as well as at stellar birth and death. They seem equally able to form out of massive accretion disks as well as from quasi-spherically collapsing plasma, which suggests that their creation is a basic byproduct of some routinely occurring ingredients. These necessary inputs seem to be rotation, collapsing or infalling/accreting plasma, and magnetic fields. Jets likely are formed at least in part from a necessity to shed the system of excess angular momentum (e.g., Meier & Nakamura 2004). The exact details of their formation, as well as the nature of the coupling between the infalling/collapsing plasma and the outflow is still an active area of controversy and research on many fronts. However, the fact that so many types of systems share this mechanism extends hope that clues gained from one class of objects can be applied to the others in the search for a unified picture.

The advantage of looking for answers in X-ray binary (XRB) jets is twofold. First, their formation seems to be a recurrent phenomenon on time scales we can observe repeatedly over the course of our own human lifetimes. For instance in the Galactic XRB GX 339–4 and Cyg X-1, accretion without observable jets proceeds into accretion with discernible jets and back again every few years (Fender 2003; Pottschmidt et al. 2003; Gleißner et al. 2004a; Homan et al.

2005). Thus the same object can provide tests of theories developed based on its earlier activity. Secondly, the existence of quality simultaneous broadband data for many sources linking the “traditional” jet outflow bands (radio and likely also infrared, or IR) and inflow bands (X-ray and optical) gives us a way of studying the relationship and interplay between the two sides of accretion. We use the word “traditional” to refer to the picture which existed up until recently that the jets and accretion flow radiate in different energy bands and can generally be studied as distinct phenomena. This picture has rapidly evolved in the last few years, beginning with the discovery of an unexpectedly intimate connection between the low and high frequency wavebands in the hard state (HS) of XRBs (see, e.g., McClintock & Remillard 2003, for a detailed definition).

Using radio observations in conjunction with 1.3–12.2 keV data from the All Sky Monitor (ASM) on-board the Rossi X-ray Timing Explorer (RXTE; Levine et al. 1996), Hannikainen et al. (1998) first discovered a near-linear correlation between the radio and X-ray emission of GX 339–4. These studies were followed by joint radio observations and pointed X-ray observations with RXTE (Wilms et al. 1999; Nowak et al. 2002). This intensive simultaneous monitoring showed that, in fact, the correlation is non-linear, with  $L_R \propto L_X^{0.7}$  (Corbel et al. 2000, 2003). Additionally, this non-linear correlation holds over orders of magnitude changes in the source luminosity with time. In fact, even after fading into quiescence, GX 339–4 seemingly returns to the same correlation in subsequent outbursts (Corbel et al. 2003), although it is not clear whether the correlation always maintains the same normalization in each instance (Nowak et al. 2005).

Electronic address: sera,mnowak@space.mit.edu  
Electronic address: j.wilms@warwick.ac.uk

<sup>1</sup> NSF Astronomy & Astrophysics Postdoctoral Fellow

Despite some possible variation in its normalization, the correlation between radio and X-ray fluxes appears to be universal to all HS XRBs with comparable broadband data (Gallo et al. 2003). The 0.7 slope of the  $\log(L_R)$ - $\log(L_X)$  correlation follows directly from analytic predictions of scaling synchrotron jet models (Falcke & Biermann 1995; Markoff et al. 2003), and can be generalized for other X-ray emission processes in terms of their dependence on the accretion rate (Heinz & Sunyaev 2003). The correlation's normalization in the  $(L_X, L_R)$  plane also depends on the central engine mass. When this scaling is accounted for, unbeamed, extragalactic, supermassive black holes sources agree remarkably well with the same radio/X-ray correlation found in Galactic, stellar-mass sources (Merloni et al. 2003; Falcke et al. 2004). The underlying physics governing the connection between the radio/IR and X-ray bands must therefore be fundamental to accreting sources regardless of mass.

In Markoff et al. (2001a) we showed that jet synchrotron emission could account for the broad continuum features of the simultaneous radio through X-ray hard state observation of the Galactic XRB, XTE J1118+480. In a later work, we showed that this same model could also explain the broad spectral features of thirteen simultaneous or quasi-simultaneous radio/X-ray observations of GX 339-4, and that the radio/X-ray correlation was naturally produced by only changing the power input into the jet (Markoff et al. 2003). These models, however, did not attempt to address the fine features present in the X-ray spectrum which are the hallmarks of an optically thick accretion disk: in particular fluorescent iron lines and a characteristic flattening above 10 keV attributed to Compton reflection (Lightman & White 1988; Ross & Fabian 1993). The reflection is generally assumed to result from a hard X-ray continuum originating above the cooler accretion disk.

We began to explore the interaction of the jet emission with the putative accretion disk in Markoff & Nowak (2004). In the hard state (HS), the spectrum is hard enough and the observed reflection signature weak enough to be problematic for coronal models where there is significant coverage of the disk by hard X-ray-emitting material (e.g., Dove et al. 1997, and references therein). Various mechanisms have been proposed to decrease both the cooling of the hard X-ray-emitting material by soft disk photons and the fraction of reflected X-rays. These mechanisms include patchy coronae (Stern et al. 1995), high disk ionization (Ross et al. 1999; Nayakshin 2000; Ballantyne et al. 2001) and beaming of the coronae away from the disk with mildly relativistic velocities (Beloborodov 1999; Malzac et al. 2001). This latter approach seems extremely close in principle to the characteristics of the base of a jet.

Compact accretion disk coronae are theoretical concepts based on observations that suggest the presence of hot electrons radiating near the inner parts of a thin accretion disk. The existence of hot electrons in the same region is also empirically required by the jets we image in the radio wavebands. The high brightness temperatures and occasionally measured linear polarization (e.g., Fender 2001) argue strongly that non-thermal synchrotron is the dominant radio-emitting process. Because the base of the jet is significantly more compact than the outer region which dominates the cm-bands, conservation arguments imply an even hotter, denser medium near the accretion disk. We therefore wish to determine whether the base of the jets can “subsume” the role of the corona. This idea was proposed already back in Fender et al. (1999), and by sub-

sume we mean provide the spectral characteristics (both direct and reflected) which are traditionally attributed to a compact Comptonizing corona. Thus we will compare coronal fits using a standard Comptonizing model (see below) to fits made by our jet model. Regardless of the ultimate relationship determined to exist between the base of the jets and the corona, this is a critical step in the road to understanding. The results of this study will provide valuable clues as to the nature of the corona, both in terms of geometrical as well as internal characteristics which differ from the base of the jets.

As an additional note, the concept of cyclo-synchrotron photons feeding inverse Compton processes in a corona has existed for over 20 years (Fabian et al. 1982), inspired by multiwavelength observations showing similar optical/X-ray behavior (Motch et al. 1982). It has recently been reconsidered for several sources (di Matteo et al. 1997; Merloni et al. 2000; Wardziński & Zdziarski 2000) in the context of magnetic flares in the corona. While a valuable step towards understanding the role of magnetic fields, these models do not address the radio emission from the jets with the same model.

The remainder of this paper is structured as follows. In Section 2 we very briefly summarize the model, with a full description included in Appendix A. In Section 3 we present our data analysis and fitting techniques, the results of which will be presented in Section 4. We discuss our conclusions in Section 5.

## 2. MODEL DETAILS

### 2.1. Jet Model Direct Emission

Our model for the jets in HS XRBs is based upon five main assumptions: 1) the total power in the jet scales with the total accretion power at the inner edge of the disk,  $Mc^2$ , 2) the jet is expanding freely and is only weakly accelerated via the resulting pressure gradient, 3) the jet contains cold protons which carry most of the kinetic energy while leptons do most of the radiating, 4) particles are eventually accelerated into a power-law distribution, and 5) this power-law is maintained along the length of the jet thereafter. These assumptions are motivated by observations which are discussed further in Appendix A, where we have also included a detailed description of the model and its development. In this section we only summarize the key parameters and assumptions of the jet model.

Beyond a small nozzle region of constant radius, which establishes the base of the jet, the jet expands sideways with the initial proper sound speed for a relativistic electron/proton plasma,  $\gamma_s \beta_s c \sim 0.4c$ . The plasma is weakly accelerated along the resulting longitudinal pressure gradient, which allows an exact solution for the velocity profile via the Euler equation (see, e.g., Falcke 1996). This results in a roughly logarithmic dependence of velocity upon distance  $z$ . After a period of more rapid acceleration immediately beyond the nozzle, the velocity gradient lessens, and the velocity saturates at Lorentz factors of  $\Gamma_j \gtrsim 2-3$ . The size of the base of the jet,  $r_0$ , is a free parameter and once fixed determines the radius as a function of distance along the jet,  $r(z)$ .

The model is most sensitive to the fitted parameter  $N_j$ , which acts as a normalization. It dictates the power initially given to the particles and magnetic field at the base of the jet, and is expressed in terms of a fraction of the Eddington luminosity  $L_{\text{Edd}} = 1.25 \times 10^{38} M_{\text{bh}, \odot} \text{ erg s}^{-1}$ . The total power input at the base of the jets is in fact approximately an order of magnitude larger than  $N_j L_{\text{Edd}}$ , due to the requirement of distributed

acceleration along the jets (see Appendix). Once  $N_j$  is specified and conservation is assumed, the macroscopic physical parameters along the jet are determined. We assume that the jet power is evenly shared between the internal and external pressures, and that the radiating particles are close to equipartition with the magnetic field. The radiating particles enter the base of the jet where the bulk velocities are lowest, with a quasi-thermal distribution. Around  $10-100 r_g$ , a significant fraction of the particles are accelerated into a power-law tail whose maximum energy is determined self-consistently with the local cooling rates.

The particles in the jet radiatively cool via adiabatic expansion, the synchrotron process, and inverse Compton upscattering; however, adiabatic expansion is assumed to dominate the observed effects of cooling because of distributed acceleration. While thermal photons from the accretion disk are included as seed photons in our Compton calculations, the beaming reduces their energy density compared to the rest frame synchrotron photons (synchrotron self-Compton; SSC), except at the very base of the jet where they can be of the same order. Reprocessed disk radiation will contribute even less and thus its feedback on the X-ray spectrum will be negligible. We therefore do not include this latter component in our calculations. In the case of near-equipartition of energy between the magnetic field and particles, inverse Compton processes only will dominate the direct synchrotron emission close to the compact object where relativistic beaming is at its minimum.

## 2.2. Accretion Disk Feedback Signatures

As the jet plasma is only weakly beamed, some fraction of the radiation will impact upon the cooler material in the accretion disk and lead to fluorescent line emission and a reflection hump (e.g., Lightman & White 1988). In Markoff & Nowak (2004) we calculated the resulting reflection spectrum for typical jet models, and found that when synchrotron emission from the acceleration region dominates the hard X-ray spectrum, the fraction of reflected emission is very small ( $\sim$ few percent). In contrast, when Compton processes (predominantly SSC) originating near the base dominate the hard X-rays, ‘reflection fractions’ of  $\lesssim 20\%$  are possible.

As discussed by Markoff & Nowak (2004), calculating the reflection spectrum for our jet models is complex, as one needs to calculate a reflected spectrum associated with each emission region along the axis of the jet. Furthermore, for our detailed jet models the disk sees a qualitatively different jet spectrum than the direct spectrum viewed by a distant observer. This is in contrast to the simple ‘moving corona’ models of, e.g., Beloborodov (1999), where both the direct spectrum and the spectrum impinging upon the disk have the same simple power law shape, and the total reflected spectrum can be calculated analytically. For the initial spectral fit studies presented here, a detailed reflection calculation for our jet model was deemed too computationally prohibitive.

For the purposes of the study presented here, we adopt a simplified approach. In our fits, we add a single Gaussian line to our continuum model, and we allow the line energy to vary between 6–7 keV and the line width,  $\sigma$ , to vary between 0–1.5 keV. We then convolve the entire *directly viewed* spectrum with a non-relativistic reflection model derived from the Green’s functions of Magdziarz & Zdziarski (1995). The amplitude of the reflected spectrum is left as a fit parameter, expressed in the usual manner as a fractional solid angle,  $\Omega/2\pi$ , subtended by the reflector. ( $\Omega/2\pi = 1$  indicates that the ra-

diation impinging upon the reflector is equal to that directly viewed by the distant observer.) This general approach of phenomenologically fitting a reflection spectrum is similar to that employed by many pure Comptonization models (e.g. Coppi 1999; Poutanen 1998), albeit here it is less likely that the directly viewed spectrum is a completely adequate proxy for the spectrum viewed by the cold disk. We will consider more sophisticated approaches to calculating the reflection features in future works.

## 2.3. Fitting Method

In our previous papers (e.g., Markoff et al. 2001a, 2003), we only compared the jet model to spectra that had been ‘unfolded’ with XSPEC using simple exponentially cutoff, broken power-law models. This is in fact the usual practice among many researchers when comparing complicated theoretical models to multiwavelength data (e.g., Esin et al. 1997; Markoff et al. 2001a). Unfortunately, such a procedure does not allow the determination of a statistical goodness-of-fit, and more importantly it does not allow one to compare the model to the fine features of the X-ray spectral density distribution (SED). Here we address this issue by forward-folding the jet model through the detector response matrices of the X-ray instrument, and then comparing to the data in ‘detector space’.

Specifically, we have imported our jet + multi-color blackbody thermal disk (similar to `diskbb`; Mitsuda et al. 1984; Makishima et al. 1986) model as a subroutine for use in standard X-ray data analysis packages. The current routine works in both XSPEC (Arnaud 1996) and ISIS (Houck & Denicola 2000). In this work, we perform our fits using ISIS v.1.2.6 as this latter package can read in and fit lower frequency simultaneous data sets (e.g., radio through optical data) as ASCII files, without the need for creating dummy response matrices. Furthermore, the ISIS ‘unfolded spectra’ (shown in the figures throughout this work) are independent of the assumed spectral model (i.e., the unfolding is done solely with the response matrix and effective area files; see Nowak et al. 2005 for details). All shown residuals, however, are for comparisons between the properly forward-folded model and the data in detector space. See Nowak et al. (2005) for a discussion of further differences between ISIS and XSPEC.

We are making detailed comparisons between our jet model and detector space data for the first time. Indeed, to our knowledge, this is the first time that such a complex, multi-wavelength model has been compared properly to the X-ray data in detector space. For this paper, we therefore have chosen to initially leave most jet model parameters free so that we can fully explore their effect on the fits. We can then determine which parameters are most fundamental for describing the data and which can effectively be frozen in future applications. This is essentially in the same spirit as prior studies with Comptonization models, where models such as `eqpair` (Coppi 1999) have significantly more parameters than are used in a typical fit. For such Comptonization models, even fairly basic parameters, such as thermal vs. nonthermal compactness (i.e., the ratio of coronal energy to coronal radius), can be degenerate with one another in real data fits, and one often chooses to freeze the nonthermal parameters to negligible values. For a detailed discussion of these points, see the review article by Coppi (2004).

Currently, our multi-component model runs significantly slower than single-component models which calculate Comptonization in the corona. Determining meaningful error bars

TABLE 1. LOG OF CYG X-1 AND GX 339-4 RXTE OBSERVATIONS

Source	Obs ID	Date	Exposure (sec.)	PCU off
Cyg X-1	40099-01-19	1999 September 25	8080	13
Cyg X-1	60090-01-26	2003 February 23	9696	1/4
Cyg X-1	60090-01-41	2003 September 22	11600	13/14
GX 339-4	20181-01-02	1997 February 10	10528	...
GX 339-4	40108-02-01	1999 April 2	9152	...
GX 339-4	40108-02-03	1999 May 14	9776	...

NOTE. — The table lists those proportional counter units (PCUs) which were off during (part of) the observation. A slash denotes a logical “or”.

for all parameters was not always possible because for some fit parameters the resulting spectrum can vary noncontinuously. Given that this is the first time that broadband data are being properly compared to our forward-folded model, such initial difficulties are not surprising. Nevertheless, the model fits presented here represent an exploration of a significant amount of the parameter space, especially given the fitting time scales involved.

### 3. DATA

We model the data from Rossi X-ray Timing Explorer (RXTE) observations for the hard state Galactic black hole candidates (BHCs) GX 339-4 and Cygnus X-1. We use data from both the RXTE Proportional Counter Array (PCA; Jahoda et al. 1996) and from the High Energy X-ray Timing Experiment (HEXTE; Rothschild et al. 1998). The data have been extracted with the recent HEASOFT 5.3.1 software release. Compared to earlier releases of this software, the relative calibration of the PCA and the HEXTE is now in excellent agreement (see analysis in, e.g., Wilms et al. 2005). Power-law fits to spectra of the Crab pulsar and nebula show the PCA data to have a systematic uncertainty of 0.5%, which we added in quadrature to the data. We used the energy bands 3–22 keV for the PCA (and grouped the data to a minimum of 30 counts/bin) and 18–200 keV for the HEXTE (where we added data from the two clusters and grouped the counts to a minimum signal-to-noise, after background subtraction, of 10 in each bin). We use the top layer of the PCA only. During part of the observations, some proportional counter units of the PCA were switched off. In these cases we added the spectra extracted for the different PCU combinations, appropriately weighting the response matrices.

The Cygnus X-1 data consist of three of the many observations taken during our several years long RXTE monitoring campaign (Pottschmidt et al. 2003; Gleißner et al. 2004a,b, and references therein) and were chosen to be representative spectra bracketing the typical hard state spectral variations of Cyg X-1. The data from GX 339-4 also have been discussed by us elsewhere (Wilms et al. 1999; Nowak et al. 2002, 2005), and bracket the typical variations in the overall hardness and luminosity of the GX 339-4 hard state. (They do not, however, encompass the most extreme bright and relatively soft HS data discussed by Homan et al. 2005, Nowak et al. 2005, and Belloni et al. 2005.) Table 1 contains a log of the observations.

In order to compare our jet models to the more standard Comptonization models, we also fit our observations with the

hybrid thermal/non-thermal Comptonization model `eqpair` (Coppi 1999). We slightly changed the publicly available version of this code to make the model run under XSPEC v.11.3.1, and hence also under ISIS v.1.2.6. To allow for a partial covering of the disk by the Compton corona, we add emission from a disk using the `diskpn` model (Gierliński et al. 1999). The peak temperature of this disk model is also set equal to the peak temperature of the seed photons input to the Compton corona. These seed photons are similarly assumed to have a spectral energy distribution that follows that of the `diskpn` model. The corona is presumed to be comprised solely of thermal electrons, and its properties are described by two parameters: a seed electron scattering optical depth,  $\tau_p$  (pair production can increase the total optical depth from this value, although pair production is negligible for the fits described in this paper), and the coronal compactness (i.e., coronal energy content divided by coronal radius), expressed as a ratio relative to the soft, seed photon compactness,  $\ell_h/\ell_s$ .

We also allow for an additive Gaussian Fe K $\alpha$  emission line whose centroid energy is constrained to be between 6 and 7 keV and whose width is constrained to be  $\sigma < 1.5$  keV. In our use of the `eqpair` model, the reflection component is relativistically smeared using the velocity profile of the `diskpn` disk model, which in turn follows the rotational velocity of a standard thin disk circularly rotating under the influence of a Paczyński-Wita pseudo-Newtonian potential (Paczynski & Wiita 1980). The reflecting medium is assumed to have solar abundances; however, the reflecting medium can be ionized, as parameterized by the ionization parameter,  $\xi$  (Done et al. 1992).

Table A4 gives the best fit parameters of these `eqpair` fits, and the fits are shown in the third column of Figs. 2 & 3. The reduced  $\chi^2$  values are close to unity, indicating very good agreement between the model and the data. The parameters found for the Comptonization model are in general agreement with those reported for earlier observations. The fits yield moderate optical electron depths of  $\tau_{es} \sim 1.5-3$  with coronal compactnesses of  $\ell_h/\ell_s \sim 3.5-8$ , which correspond to coronal temperatures of  $\sim 25-100$  keV. (Note that the  $\tau_{es} \sim 6.7$  for Obs ID 40108-02-03 has rather large error bars, and is partly being driven by the poor statistics in the HEXTE band.)

All of the coronal model fits yield reflection covering fractions  $\lesssim 20\%$ . None of the fits strongly require ionized reflection; however, the reflection model used by the `eqpair` code is very simplified (being based upon the `pexriv` code; Done et al. 1992). The fitted equivalent widths of the Fe K $\alpha$  lines are on the order of 150 eV, and consistent with the highly smeared reflection models employed, the lines are generally found to be rather broad. As will be discussed elsewhere in more detail (Wilms et al. 2005), we believe that part (although not all) of the fitted line broadness is caused by the Comptonization model employed here having too simplified a description of the transition between the accretion disk emission and the Comptonization continuum. Finally, the changes in accretion disk temperature and flux, coupled with the changes in coronal compactness and optical depth, are in response to the fact that we have deliberately chosen observations that span a wide range of flux and spectral hardnesses.

Detailed discussions of coronal model fits to Cyg X-1 data (e.g., comparison to phenomenological broken power-law fits, comparison to timing data) are discussed in Wilms et al. (2005). Their are three main points that we wish to emphasize with the fits presented here. First, the `eqpair` fits

describe the data well – as well as any coronal models that we have explored (although not better than simple exponentially cutoff, broken power-law models; Nowak et al. 2005; Wilms et al. 2005). Second, the fits do not require comparatively as large reflection fractions<sup>2</sup>. Third, and related to the previous point, the coronal models themselves describe a continuum spectrum more complicated than a simple, exponentially cutoff power-law. Some fraction of the spectral hardening above 10 keV, normally attributed to the ‘reflection hump’, is in fact described by curvature of the Comptonization continuum. In Compton coronal models, this curvature is in part due to transiting from a spectrum strongly affected by the soft seed photons to one strongly dominated by photons that have been multiply Compton scattered. As we discuss below, this continuum curvature an additional interpretation in jet models.

#### 4. JET MODEL RESULTS

As mentioned above, our strategy in testing our jet models against the data was to allow the maximum number of model parameters to vary freely during the fit. This allowed us to explore which parameters had the greatest influence on the fits. Several parameters settled on fairly similar values for both sources and all observations, which suggests that those parameters could be fixed in future applications of this model. We will discuss this possibility explicitly below.

Fits with a complicated model can easily lead to false, local minima; therefore, we began the fitting procedure outside of *ISIS*, using unfolded data sets in order to find a set of starting parameters that would yield reduced  $\chi^2 \lesssim 5$ . For this paper we have chosen to explore only models with rough equipartition between the magnetic and radiating particle pressures ( $k \approx 1$ ). This assumption is obviously not applicable for Poynting flux dominated jets; however, we consider the very weak acceleration required by observations to be an indication that magnetic domination (which would generally imply stronger acceleration mechanisms) is not likely to be very extreme.

We use the results of Markoff & Nowak (2004) as a rough guide for consistency, and only consider models with reflection fractions  $\lesssim 20\%$  for jet nozzle radii  $r_0 \lesssim 20r_g$  to be ‘successful’ fits. For smaller values of the radii, slightly lower values for the reflection fraction would be expected. In all cases the jet models seemed to naturally prefer reflection fractions  $\Omega/2\pi \lesssim 20\%$ , so in practice this restriction on reflection fraction was not an issue.

Fig. 1 shows a representative model for GX 339–4 in order to illustrate the contribution from the various components which go into the later figures showing actual fits. The radio through IR originates exclusively from self-absorbed synchrotron radiation beginning at  $z_{\text{acc}}$  and continuing outwards along the jet. Optically thin synchrotron emission from the accelerated power-law tail of leptons also contributes to the soft X-ray band. The base of the jet radiates direct synchrotron photons, giving a slight hump in the optical/UV, which are then included as seed photons (along with disk photons) for upscattering by the emitting electrons into an SSC/EC “hump” in the hard X-rays. The shape of this hump

is rounded, due to the quasi-thermal particle distribution assumed in the base, and thus reduces the need for a large fraction of disk-reflected photons to contribute to the spectral break/hardening at  $\sim 10$  keV. The possibility that there are two correlated continuum components in the X-ray band is supported by our ensemble of simultaneous radio/X-ray observations of Cyg X-1, whose spectra are very well-described by exponentially cut-off, broken power-laws (Nowak et al. 2005; Wilms et al. 2005). In these models, the soft X-ray spectral slope is very well-correlated with the break of the hard X-ray spectral slope, and the hard X-rays are very well-correlated with the radio (Gleißner et al. 2004a; Nowak et al. 2005). The multicolor blackbody included in the jet model is also shown in the soft X-ray band. The photons from this component are included in the inverse Compton upscattering within the jet.

The statistical fits are shown in Figs. 2 & 3, for GX 339–4 and Cyg X-1, respectively. Each figure encompasses nine panels, with each row representing a single simultaneous radio and X-ray observation of the source. The first column shows the entire radio through X-ray jet model + soft disk + reflection fit, and the second column focuses just on the X-ray band. The last column shows the thermal Compton corona model from *eqpair* for comparison. Values for all fitted parameters are given in Tables 2–4.

The results presented in Figs. 2 & 3 and Tables A2, A3, & A4 immediately demonstrate three important results of this work.

- **Jet models describe the data equally well as pure Compton corona models, even when employing the broad-band and high statistics of the RXTE data.** There has been question in the literature (e.g., Zdziarski et al. 2004) as to whether or not jet models can adequately describe the spectral cutoff of the hard tail. While pure synchrotron jet models may not be able to describe the steep cutoff present in some (but not all) observations, jets can also successfully account for this hard tail cutoff via Comptonization. The primary differences between ‘traditional’ coronal models and jet coronal models are that the coronal temperatures are higher in the latter ( $\sim 10^{10}$  K vs.  $\sim 10^9$  K), and the disk seed photons in jet models are significantly augmented—if not dominated—by synchrotron seed photons.
- **The jet models, similar to the Compton corona models, describe a complex continuum with curvature – specifically, a hardening above 10 keV.** Again, the hardening often predominantly ascribed to a ‘reflection hump’ is being somewhat subsumed by continuum emission. In the jet model, the steeper slope of the soft X-rays is primarily due to synchrotron emission from the jet, rather than being influenced by the disk photons, while the hardening is due to the SSC/EC component. Reflection is present, but represents a smaller fraction of the total hard flux compared to the corona models. Note that the fits discussed here are in contrast to earlier incarnations of the jet model which attempted to describe observations solely via the synchrotron component (e.g., the studies of XTE J1118+480; Markoff et al. 2001a). For XTE J1118+480, the lack of any discernible break or hardening near 10 keV in the continuum spectrum was used to argue for the lack of a reflection component (Miller et al. 2002), which would be consistent with

<sup>2</sup> The *pexriv* model, incorporated into the *eqpair* model, tends to have an unnaturally sharp ionized Fe edge structure, especially when compared to the more sophisticated models of Ross & Fabian (2005). The reflection fraction can be artificially depressed when employing the *pexriv* model, so as to minimize residuals from its sharp ionization edge. However, as we employ a large degree of relativistic smearing, and hence smooth out the edge, we do not expect to be subject to this systematic effect.

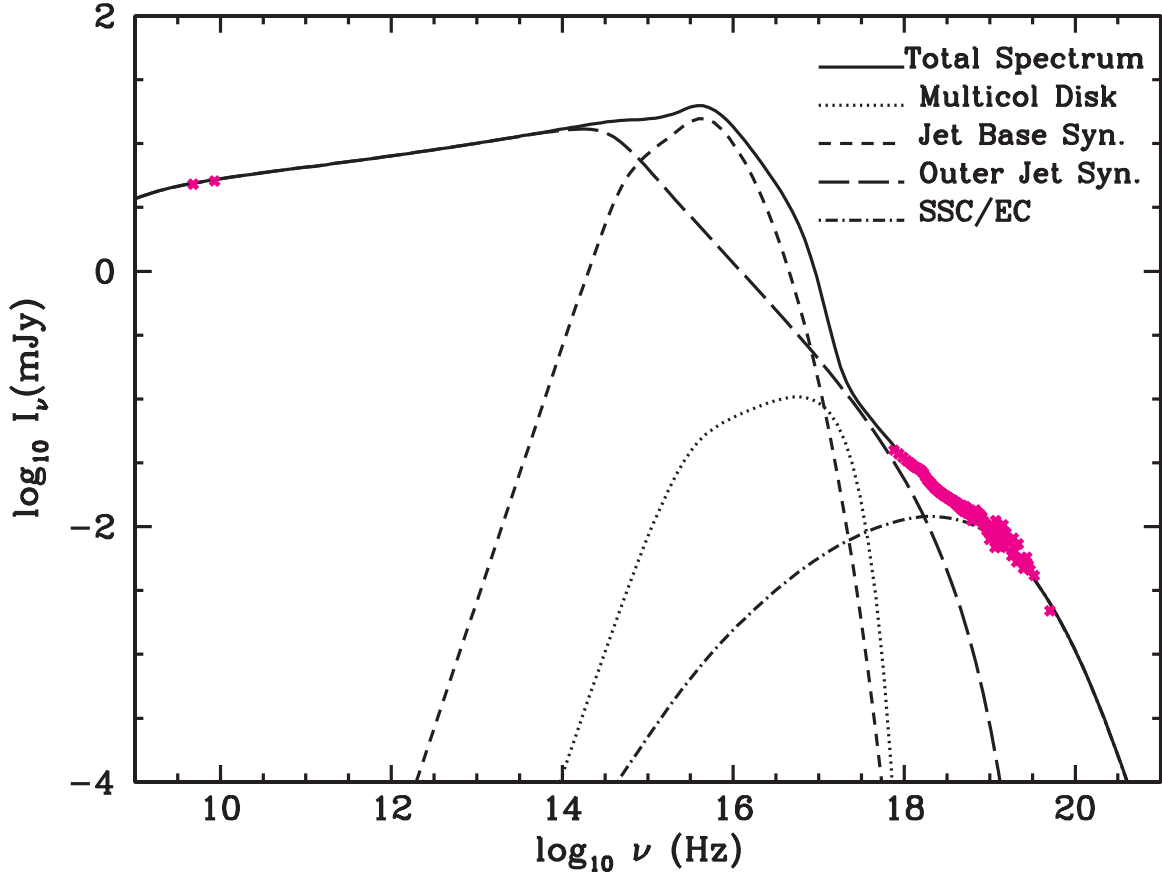


FIG. 1.— Representative model for GX 339–4 obs.id. 40108-02-01, showing jet and multi-color blackbody models only. This is the model which is then convolved with the disk reflection and line emission elements for the final statistical fit. The components are labeled.

a jet spectrum dominated by the synchrotron component (Markoff et al. 2001a; Markoff & Nowak 2004). In contrast, the fact that all of the XRB spectra shown here harden above 10 keV argue for the importance of both the synchrotron and SSC/EC components of the jet spectrum for these fits, as well as the presence of reflection.

- **Although the jet and Compton coronal models describe the X-ray data equally well, only the jet model naturally describes both the amplitude and slope of the radio data without the need for additional free parameters.** It is important to note that the radio spectrum, as well as the bulk of the 3-200 keV X-ray continuum (i.e., the overall amplitude and continuum curvature), are almost solely driven by the parameters of the jet: energy input to the jet ( $N_j L_{\text{Edd}}$ ), radius of the jet base ( $r_0$ ), electron temperature at the jet base ( $T_e$ ), slope of the power-law component of the electron energy distribution ( $p$ ), the equipartition parameter ( $k$ ), and the location of the particle acceleration zone in the jet ( $z_{\text{acc}}$ ). If one begins instead with a corona model and attempts to fit the amplitude and slope of the radio data by assuming a relationship to an extant jet model, this will in essence require the addition of many more parameters to describe just two physical quantities. We argue that nothing can be gained by this approach, which is why we have chosen to study the test case of full coupling.

From our set of jet model fits that successfully describe the

GX 339–4 and Cyg X-1 data, we can now explore the implications of the fitted parameters. Cyg X-1 and GX 339–4 are somewhat different sources while in their hard states. The luminosity of GX 339–4 varies much more than that of Cyg X-1. This is apparent in the fitted values for the power normalization  $N_j$  and output power  $L_j$  shown in the first two columns of Table A2. Both sources show best fit  $N_j$  in the range of  $10^{-4} - 10^{-3} L_{\text{Edd}}$ , but GX 339–4 shows significantly more variation in this parameter. Differences can also be seen in the other main parameters, for instance on average GX 339–4 favors slightly larger values of the nozzle radius,  $r_0$ . This reflects the slightly higher ratio of X-ray to radio flux observed in Cyg X-1. A smaller scale jet base, for a given jet power, increases the jet compactness which in turn gives a slightly higher flux (with the X-ray flux being more sensitive to this effect) and pushes all jet emission to slightly higher frequencies.

Other fit parameters also indicate differences between these two sources; however, the parameters surprisingly fall roughly in the same range given the *a priori* possibility for much greater parameter variations. Note that the lowest luminosity GX 339–4 observation, Obs ID 40108-02-03, has poor enough statistics that the following general statements about the GX 339–4 fits will be based mostly on the brighter two observations. For example, both the electron temperature,  $T_e$ , and the location of the start of the acceleration zone,  $z_{\text{acc}}$ , tend to be larger in GX 339–4 than in Cyg X-1. (Although we were unable to find adequate error bars for the latter parameter, the

trend of finding larger values in GX 339–4 was persistent.) Additionally, we note that the electron power law index,  $p$ , shows more variation in GX 339–4 than in Cyg X-1.

Although the range in electron temperatures at the base of the jets falls within a range of a factor of  $< 2$  for both sources, one of the criticisms of this class of models has been that  $\sim 3\text{--}5 \times 10^{10}$  K is not as “natural” a value as the  $\sim 100$  keV typically used in thermal Comptonization models. The jet model electron temperature, however, is comparable to or slightly greater than the value typically derived for radiatively inefficient accretion flows (e.g., Narayan et al. 1998). If some fraction of the accreting plasma is fed directly into the jets, and also perhaps heated slightly in the process, we would expect such a temperature.

On the other hand, several jet model free parameters seemed to settle quite quickly into similar values for both Cyg X-1 and GX 339–4: the equipartition factor  $k$ , the fraction of accelerated particles  $pl_f$ , and the ratio of nozzle length to radius  $h_0$ . Physically, this suggests that these jets either are close to equipartition, or we have found a local minima of solutions for  $k \approx 1\text{--}2$ , and we may find other reasonable minima for  $k \gg 1$ , e.g., magnetically-dominated jets. We plan to explore this particular question in a future work. It seems reasonable, however, to freeze the fraction of accelerated particles at  $\sim 75\%$  and make the statement that reasonably efficient acceleration is expected to occur in hard state BHC jets. Similarly, a compact base/corona region with scale height similar to the radius seems a reasonable assumption. It is likely that this parameter can also be frozen in future applications of the jet model.

We listed the two “acceleration parameters”, the shock speed relative to the bulk plasma flow,  $u_{\text{acc}}/c$ , and the ratio of the scattering mean free path to the gyroradius,  $f_{sc}$ , as separate fit parameters. However, as discussed in the Appendix, these parameters are perhaps not physically meaningful as currently defined, since we are no longer as convinced that the acceleration process is diffusive Fermi acceleration. These parameters enter into the acceleration rate as the factor  $f = (u_{\text{acc}}/c)^2/f_{sc}$ , which is compared to the sum of the cooling rates from synchrotron and inverse Compton radiation, and adiabatic expansion in order to calculate the local maximum accelerated lepton energy. Therefore, this parameter can be loosely interpreted as a factor related to the efficiency of the acceleration process and merged for future fits into a single parameter. For the current fits, the individual components were left free to vary, with mixed results. For Cyg X-1,  $f \approx 2\text{--}3 \times 10^{-4}$ , suggesting a meaningful range of fits. However, for GX 339–4,  $f$  ranges over two orders of magnitude, and we suspect that we did not fully explore parameter space meaningfully for this source. In future applications of the model, it is likely that we will combine these two parameters into a single parameter that will absorb our uncertainty about the acceleration process.

While we list best fit values for the multicolor blackbody disk model parameters  $L_{\text{disk}}$  and  $T_{\text{disk}}$ , as well as the derived inner radius  $r_{\text{in}}$ , it is important to keep in mind that because the data only extend down to a few keV, we cannot meaningfully constrain this component from spectral fitting. As described in the Appendix, the disk photons are not as important to the overall photon field as the locally produced synchrotron photons and thus can mainly be constrained by their direct spectral contribution. This contribution, although weak, is in fact required for a good fit, but it is not unique. Ibragimov et al. (2005) have also fit some of the X-ray data presented here, and

for similar reasons fixed the thermal disk parameters. On the other hand, for the disk emission plus Comptonization models presented here (as well as for those presented in Wilms et al. 2005), the temperature of the disk was tied to the temperature of the seed photons—i.e., the thermal photons were the *only* source of seed photons for Comptonization. Thus by virtue of these imposed restrictions, much more stringent formal limits for the disk components were attainable.

The main result to take away about the accretion flow modeling is that our fits are generally consistent with a sub-Eddington accretion disk with temperatures somewhat less than 1 keV. Similarly, the total power entering into the jets is roughly consistent with being of the same order as the observed luminosity required in the disk to be consistent with the data. The presence of a weak disk component is necessary for a good fit, and thus disk photons will contribute to the inverse Compton component from the jet. We do not, however, feel we can confidently make any statements about the disk geometry and thus the accretion rate at the inner radius assumedly feeding the jets.

For both GX 339–4 and Cyg X-1, the amount of reflection required by the jet models is roughly comparable to, although in general slightly lower than, that required by Comptonization models. This trend can be understood by the fact that the jet base SSC/EC component dominates above 10 keV, and to some extent subsumes the role played by the “Compton hump” normally attributed to disk reflection. This effect of course brings up an interesting point: there is a clear degeneracy in how the spectral hardening above 10 keV can be understood in terms of continuum models. The fact that the jet SSC/EC component has a similar appearance to the Compton reflection hump does not preclude the presence of both. Clearly, the fluorescent Fe line implies that there must be a degree of reflection. What these results (as well as the Comptonization fits; Wilms et al. 2005) do suggest is that one cannot uniquely determine a reflection fraction independently of the presumed continuum model.

## 5. DISCUSSION AND CONCLUSIONS

The key result of this work is that we have clearly demonstrated that even the high statistics of RXTE X-ray data cannot distinguish between the jet model and thermal Comptonization. (Indeed, the RXTE data also cannot distinguish between thermal and nonthermal Comptonization models, as has been previously discussed by, e.g., Coppi 2004). In this sense, the base of the jets can be said to effectively “subsume”, at least spectrally, the role created for the corona. The main difference between these two pictures then comes down to geometry, inflow versus outflow, and the relationship of the corona to the lower-frequency-radiating regions of the outer jets. The jet model presented here is consistent with the physical picture seen in relativistic MHD simulations (Miller & Stone 2000; Hawley & Krolik 2001; Meier & Nakamura 2004), where the corona is not static but instead is a windy hot material blowing away from the inner regions of the accretion flow. This wind/corona is likely what enters into, or is collimated and becomes, the jets and therefore it is intimately related to the larger scale outflows, similar to what we propose here. In addition, the jet base provides a natural illuminator for the disk.

Our ability to constrain the role of the accretion disk is significantly limited by the lack of low-energy data. Ideally we would like to be able to determine the inner temperature, and perhaps also assess the need for a recessed inner edge, explicitly from the observations. Having this information would al-

low us to better constrain the ratio of external to synchrotron-produced photons in the jet base. Additionally, we expect differences between jet models and Compton corona models to become more pronounced as one considers data above the nominal Comptonization cutoff at 100–200 keV. From both of these perspectives, the observational situation will likely soon improve with the launch of ASTRO-E2, which will have the ability to observe from 0.5–600 keV and thus more stringently constrain both jet and Compton corona models. Additionally, although the broad-band effects of reflection, e.g., the reflection hump, cannot be fit independently from the assumed continuum, there is some hope that finer spectral resolution (perhaps coupled to correlated studies of the continuum variability) will be able to more uniquely determine the reflection fraction based upon detailed modeling of the Fe line (Young & Reynolds 2000; Ross & Fabian 2005).

In the scenario considered here, the nozzle/base of the jet is the dominant region for the creation of the hard X-ray emission via Comptonization processes. Constructing a completely realistic description of this region, however, is difficult given that the physics of jet formation, acceleration, and collimation are not yet understood. The nozzle essentially represents the initial conditions which fix parameters along the rest of the jet. We have shown that the form we have developed for this region over the last several years can successfully mimic the corona in purpose, but it is not as well-determined feature as we would like. An alternative, but also currently rather ad-hoc, possibility would be to invoke special conditions linking an outflowing corona with more typical thermal plasma conditions to an outer jet. This would require some kind of acceleration and/or heating of the particles at the interface (and thus more free parameters), but may satisfy many of the spectral requirements.

One possible way to discern between these two situations, or at the very least limit the possible flux from a nozzle, could be to calculate the amount of local ionization expected from nozzle UV photons and compare that to what is observed (J. Krolik, priv. comm.). If it can be shown for a given source that all observed line emission can be accounted for by the known companion, this limit may be rather stringent. We note, however, that in High Mass X-ray Binaries such as Cyg X-1, the companion luminosity, especially in the UV, is extremely high. It is therefore more likely that meaningful limits can be obtained for Low Mass X-ray Binaries, such as GX 339–4.

While we have focused on modeling simultaneous radio/X-ray data sets in this paper, for GX 339–4 and several other sources observations do exist which in addition have simul-

taneous IR/optical data. Near-IR data in particular can provide a valuable constraint on the jet synchrotron component, especially when the transition turnover from optically thick to thin is resolved (e.g. Homan et al. 2005). Using the work presented here as groundwork, we will explore elsewhere whether more parameters can be constrained by such data sets. Similarly, with *HESS* already online and *GLAST* imminent, predictions of  $\gamma$ -ray fluxes will be another important way of testing not only the current model, but models which incorporate hadronic processes.

However, the next major frontier for application of our jet model clearly is to consider questions of time-dependence. By studying the lag between the radio and X-ray correlated variability, we can constrain the plasma speed and/or distance between the two regions. The existing radio/X-ray flux correlations constrain the long time scale, while simultaneous radio/RXTE pointed observations constrain thousand of second time scales (Gleißner et al. 2004a). We are currently using long duration (several hundred ksec), quasi-continuous radio/X-ray observations of Cyg X-1 to explore intermediate time scales (Markoff et al., in prep.). The models considered here, however, are steady-state and focus on the hard accretion state only. Some of the most interesting and revealing behavior is seen during transitions between these states. For instance, during transition into the hard state we observe a hard X-ray tail before the jet forms as a detectable radio structure (Nowak et al. 2002; Miller et al. 2004). The presence of the tail suggests that the jet base/corona may form as a viable region before the outer stable radio-emitting structures are built up. There are also significant clues coming from noise and faster scaled time variability such as QPOs Homan & Belloni (2005) which need to be integrated into the picture. In general the state transitions reveal many interesting properties which are clearly not due to a steady state model, but which do share several similar properties to the more persistent hard states. Studying the time-dependent behavior of these systems will likely be an effective way to further constrain the conditions at the jet base/corona.

We acknowledge partial funding and travel grants from the Deutscher Akademischer Austauschdienst (DAAD) and the National Science Foundation, under NSF grant INT-0233441. M.A.N. is also supported by NASA Grant SV3-73016. S.M. is supported by an NSF Astronomy & Astrophysics postdoctoral fellowship, under NSF Award AST-0201597. We thank the Aspen Center for Physics for its hospitality during the final stages of the preparation of this paper, as well as the anonymous referee for helpful comments.

## APPENDIX

### DETAILED DESCRIPTION OF THE JET MODEL

#### *Background*

Like all models for optically thick outflows, our jet model builds on the initial work of Blandford & Königl (1979). Their paper demonstrated how a superposition of idealized, self-absorbed, conical jet components results in a flat synchrotron spectrum in the radio bands. In reality, compact jets usually deviate from this idealized case, and show a slight spectral inversion in the radio wavebands, with spectral index  $\alpha \sim 0.0 - 0.2$  ( $F_\nu \propto \nu^\alpha$ ). A more realistic treatment of the internal physics can account for this inversion. Using the framework for hydrodynamical jets developed in Falcke & Biermann (1995), Falcke (1996) developed a “free jet” model which is more self-consistent. For instance, the assumption that the jet is roughly conical via lateral expansion with a constant sound speed requires weak longitudinal acceleration. The Euler equation can then be solved for the longitudinal velocity gradient, assuming only adiabatic losses, and is analogous to a pressure driven wind solution with the proper jet speed replacing the wind speed. This weak acceleration combined with relativistic beaming effects will result in the spectral inversion typical of compact jet sources.

These earlier models were very useful for studying the general physical scalings predicted by compact jet models. However, without full particle distributions and radiative transfer, they cannot be tested against observed spectral data. Our models have



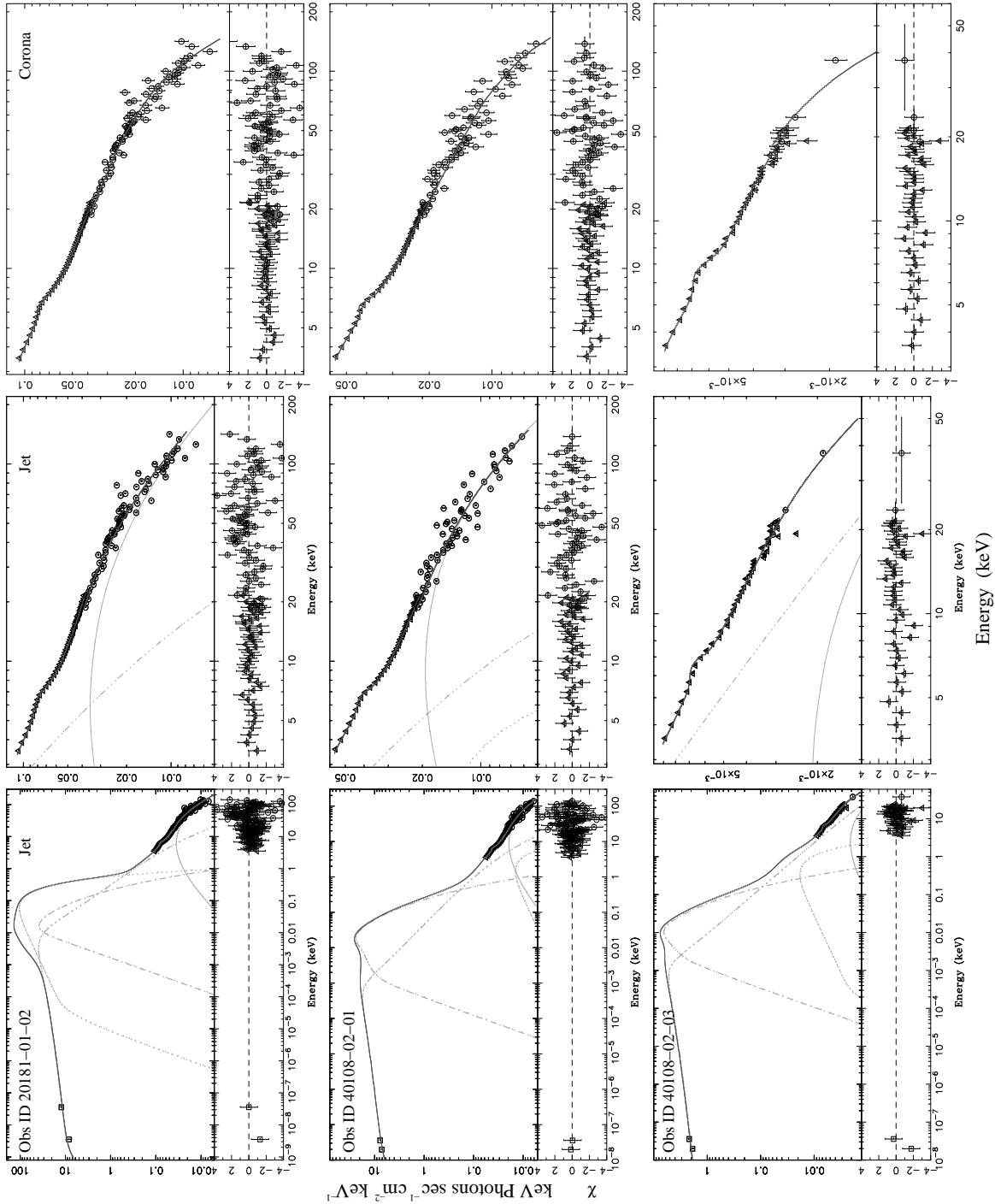


FIG. 2.— Jet and corona model fits to radio and X-ray data of GX339-4, with individual spectral components for the jet model shown in grey. In each panel, synchrotron from the jet pre-shock region is shown as a dot-dash line, synchrotron from the post-shock region is shown as a dash-triple dot line, synchrotron self-Compton plus external Compton is shown as a solid line, and the disk radiation is shown as a dotted line. The panels are laid out as follows. From bottom to top (left to right on the figure), the fits are with the `mfjet` model (radio/X-ray and X-ray data) and then the `qpair` model. From left to right (top to bottom on the figure), the ObsIDs are 20181-01-02, 40108-02-01, and 40108-02-03. The spectra are shown as model-independent unfolded spectra; however, the fits and residuals are from the properly forward-folded models.

been developed on the basis of these earlier papers, but specifically focus on the problem of spectral predictions. These models are only appropriate for systems where the jets are not expected to be highly collimated nor highly accelerated, e.g., the jets in hard state XRBs and LLAGN.

### Jet Physical Parameters

We start by assuming that the base of the jets are at the speed of sound for a relativistic gas with adiabatic index  $4/3$ , giving a proper sound speed  $\beta_s \gamma_s \sim 0.4$ . Furthermore, we assume the jets expands laterally with the constant sound speed, which is appro-

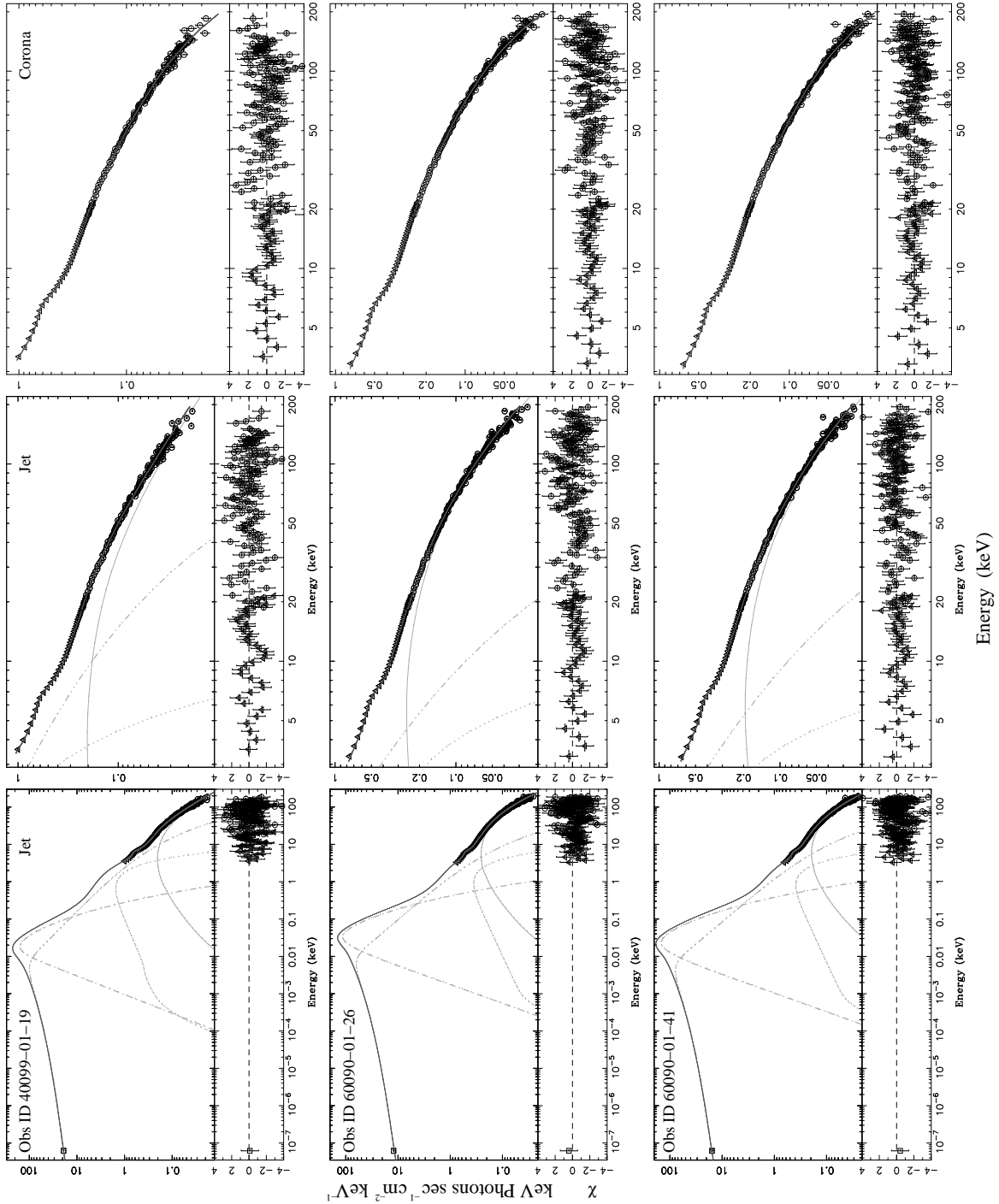


FIG. 3.— Same as Fig. 2, except for Cyg X-1 data. From left to right, (top to bottom), the ObsIds are 4099-01-19, 60090-01-26, and 60090-01-41.

appropriate under the assumption of maximally efficient jets (see Falcke & Biermann 1995). The resulting longitudinal acceleration along the axes is largest near the bases, and asymptotically approaches a maximum of Lorentz factor  $\gamma_j \sim 2-3$  in the outer radio emitting regions, and  $\gamma_j \lesssim 1.5$  for the synchrotron emission. Such weak beaming factors are suggested by observations of hard state jets (Maccarone 2003; Gallo et al. 2003), in contrast to the near light-speed velocities implied by superluminal motion in higher luminosity radio-emitting states.

The main free parameters of this model are the power normalization  $N_j$ , the radius of the jet nozzle  $r_0$ , the equipartition of energy between the radiating leptons and the magnetic field  $k = U_B/U_e$ , and the parameters determining the initial lepton distribution as described below. We also left the length of the nozzle region (with fixed radius),  $h_0$  free, but it turns out the fits are not very sensitive to its value. Other parameters which come in, such as the central mass  $m_{bh}$ , the inclination of the jets to the line of sight  $\theta_i$  and the distance to the source  $d_{kpc}$ , are determined from observations and remain fixed for any given source. Finally

there are two parameters related to the presence of weak disk emission, the total luminosity radiated by the disk and its inner radius temperature,  $L_d$  and  $T_{in}$  respectively. These cannot be well constrained by our data because although they are spectrally fit assuming a multi-color disk blackbody (Mitsuda et al. 1984; Makishima et al. 1986), the low-energy X-ray spectrum is not well covered in our observations. Similarly, although they do contribute to the photon field upscattered by energetic jet leptons, they are not the dominate component.

The most important free parameter is  $N_j$ , parameterized in terms of the Eddington luminosity, which determines the power initially input into the particles and magnetic field at the base of the jets. The total power input at the base of the jets is in fact approximately an order of magnitude larger than  $N_j L_{Edd}$ , and for our model can be estimated only *a posteriori* from the resulting emission in the emitting rest frame. The difference between  $N_j L_{Edd}$  and the total output radiation  $L_j$  expresses the lack of knowledge of what initially collimates the nozzle, as well as what causes the distributed reenergization—and consequent energy requirement—to maintain the observed (e.g. Jester et al. 2001) particle distributions along the jet (see below).  $N_j$  plays a similar role to the compactness parameter in thermal Comptonization models, which parameterizes the total energetics in the absence of an understanding of the mechanism for energizing the corona (Dove et al. 1997; Coppi 1999),

As a consequence of assuming maximal jets, there should be approximate equipartition between the kinetic and internal energy. Once  $N_j$  is fixed, therefore, the energetics along the jets are fixed as well. For a given  $r_0$  and  $k$  at the base, conservation of energy and particle flux together with the proper velocity profile along the jet,  $\gamma_j(z)\beta_j(z)$ , determine the radius, density, and magnetic field profiles along the entire jets. What is left to be determined is how the energy in the radiating particles is distributed.

### *Radiating Particle Distributions*

As mentioned earlier, we assume that the jets contain both leptons and hadrons, but that the hadrons remain non-relativistic and serve only to carry the bulk kinetic energy. The leptons, which are assumed to be mildly relativistic and quasi-thermally distributed (see, e.g., Quataert & Gruzinov 1999) are thus more likely to be accelerated. In any case, we assume that leptons are predominantly responsible for the observed radiation. This is begging the question of hadronic acceleration, because the end effect of significant hadronic acceleration and subsequent inelastic collisions will invariably be relativistic leptons. The expected energy distributions, whether from direct acceleration or creation via hadronic collisions, are not trivial to discern from X-ray emission alone. Therefore we do not specify whether the radiating particles are electrons or positrons, since this will not effect the observable outcome. Eventually the consistency with these results can be checked against hadronic models, but this is a very difficult problem (see, e.g. Mannheim 1993; Markoff et al. 1999; Böttcher & Reimer 2004) and is not considered here. The one hint for what will be required beyond neutral matter is that we do not require  $n_e/n_p = 1$ , and once a fit is made, we can see if additional pair creation is necessary.

The current model was developed in simplified form by Falcke & Markoff (2000), where we first incorporated simple particle distributions for the radiating leptons and calculated the radiative transfer along the jets. Our goal was to determine if the same kind of model which could explain the inverted radio core of the Galactic Center supermassive black hole, Sgr A\*, also predicted significant X-ray emission. This idea was motivated by the first identification of Sgr A\* in the X-ray band by the *Chandra* Observatory (Baganoff et al. 2003). We explored two “canonical” types of particle distributions, power-laws and Maxwellians, for Sgr A\* in its quiescent state (see, e.g., Melia & Falcke 2001). These two ostensibly different distributions result in similar fits as long as the characteristic particle energy, ( $\gamma_{e,min}$  for the power-law or  $\gamma_{e,peak}$  for the Maxwellian) is similar. Unlike “typical” low-luminosity AGN (LLAGN; Ho 1999), the quiescent Sgr A\* does not show any indication of a power-law of optically thin synchrotron emission after the break from its flat/inverted radio spectrum. Therefore if the radiating particles have a power-law distribution, it must be so steep as to be indistinguishable from a Maxwellian in the optically thin regime. Either scenario strongly suggests, for example, that acceleration in the jets of Sgr A\* is absent or very inefficient at  $L \sim 10^{-9} L_{Edd}$ .

Based on Sgr A\*, we therefore assume that the baseline particle distribution, below a certain accretion rate which must be very low, is quasi-thermal. This scenario is consistent with particles being advected into the jets directly from the accretion flow, or created and roughly thermalized near the base. Sources with jets at higher luminosity, such as AGN and XRBs, do, however, show the standard indicator of particle acceleration: optically thin synchrotron emission from a power-law distribution of particles (e.g., Marscher & Gear 1985; Fender & Kuulkers 2001, and refs. therein). Interestingly, Sgr A\* shows daily flaring in which the X-ray spectrum rapidly increases in flux and hardens dramatically (Baganoff et al. 2001; Baganoff 2003). The flare emission stems from energization of the particles via acceleration, heating or both at once (Markoff et al. 2001b), resulting in enhanced synchrotron and/or SSC emission in the X-rays. Because the increased X-ray flux during the flares brings Sgr A\* more in line with typical levels of LLAGN activity (Markoff 2005), one interpretation is that acceleration of particles is the main factor contributing to the comparative weakness of Sgr A\*. We also therefore assume that above some critical accretion rate above that of Sgr A\*, particle acceleration will be commonplace in the jets. This is also necessary to explain the high synchrotron efficiency in XRBs (see, e.g., Markoff et al. 2003).

In the only XRB where the optically thick-to-thin turnover from compact jet synchrotron has been directly observed (GX 339–4; Corbel & Fender 2002; Homan et al. 2005), it occurs at a significantly lower frequency than would be expected if the acceleration began in the jet base. We therefore assume that when particle acceleration occurs, it begins at some location  $z_{acc}$  along the jet, which is a free parameter but which appears to fall in the range of a few  $10 - 10^2 r_g$  for most sources we have so far considered. The fraction of particles accelerated into the tail is a free parameter in our model, but is generally driven to fairly high values so we will likely fix it at some value above 80% in future applications. The power-law index of the tail  $p$  ( $N(E) \propto E^{-p}$ ) is also a free parameter, and can be constrained by the data.

Particle acceleration must compete with radiative and adiabatic cooling to energize the quasi-thermal particles into a power-law tail. Where the sum of the cooling rates equals the acceleration rate defines the maximum achievable particle energy,  $\gamma_{e,max}$ . Unfortunately since the acceleration process is still an open question, the acceleration rate is open to significant interpretation. In Markoff et al. (2001b) and Markoff et al. (2001a), we used acceleration rates appropriate for diffusive shock acceleration in the

most conservative case of the magnetic field direction parallel to the shock normal (see Jokipii 1987). The rate of diffusive shock acceleration is always proportional to the magnetic field. If synchrotron cooling dominates the cooling term,  $\gamma_{e,\max}$  will thus be independent of the magnetic field and can give information about the plasma parameters if the location of the cutoff can be determined. In Markoff et al. (2001a) we showed that this results in a synchrotron emission cutoff around 100 keV for  $\beta_{\text{sh}} \gtrsim 0.5$  and if the ratio between the particle's mean free path for diffusive scattering to the gyroradius,  $\xi = \lambda/r_B \approx 100$ . In general  $\xi$  is thought to be limited by the ratio of the particle to shock velocities, and so likely no higher than  $10^2 - 10^3$ , but this value is certainly not fixed.

At the time of writing, other processes such as stochastic resonant acceleration (e.g., Miller 1998) are coming into favor. Given this uncertainty in the mechanism, we are loosening the constraints on the acceleration rate we used previously and are letting  $\xi$  and  $\beta_{\text{sh}}$  vary. If the acceleration rate we are using is not really physical, then these parameters have lost their meaning and become essentially fudge factors absorbing the free parameters controlling the acceleration rate for other mechanisms, to be determined later. If shock acceleration does still hold, then these tell us about the plasma conditions in the jets.

Regardless of the process, the inferred cooling times for the accelerated leptons will be too high to maintain the power-law along the jets unless there is continuous distributed acceleration. Distributed, continuous *in situ* injection is a standard requirement for explaining the persistence of particle distributions along AGN jets (Jester et al. 2001) and seems to be a common feature in outflows.

So to summarize the particle distribution discussion, we assume that the particles enter the jet with a relativistic quasi-Maxwellian distribution, the temperature of which,  $T_e$ , is a fitted parameter. Some fraction of the particles are then assumed to be accelerated continuously beyond a location in the jets,  $z_{\text{acc}}$ . Where exactly can be constrained by the frequency of the optically thick-to-thin break in the synchrotron spectrum, if detected, as well as from the synchrotron component contributing to the soft X-rays.

### *Jet Continuum Components*

As the leptons travel outwards along the jets, they interact with the local magnetic field and photon fields and cool via synchrotron and inverse Compton radiation. Inverse Compton processes are strongest near the base of the jets, where the density is highest, and thus one X-ray component is due to the upscattering of both jet synchrotron photons as well as thermal disk photons by the quasi-thermal leptons in the base. For the assumptions in this paper (the thin disk is recessed with inner radius  $r_{\text{in}}$  calculated from fitted parameters  $L_d$  and  $T_{\text{in}}$ ), the disk thermal photon field is only an important factor at the very base of the jets. This is because even the mild beaming in the jets quickly serves to weaken the disk photon field's energy density compared to the locally produced synchrotron photons.

Once the acceleration zone is reached, it is difficult to suppress X-ray synchrotron radiation from the tail of accelerated leptons in the diffusive acceleration case (see Markoff et al. 2001a). As described above, we are relaxing the constraint on the synchrotron cutoff by allowing for an alternate acceleration process. In this scenario, a power-law of synchrotron radiation will contribute significantly at least to the soft X-ray band, but not necessarily to the hard X-rays which are in this model dominated by inverse Comptonized disk and synchrotron photons.

This distinction is important because, as shown by Markoff & Nowak (2004), a very typical hard state model where the X-rays are exclusively due to synchrotron radiation cannot easily reproduce disk reflection fractions greater than a few percent (assuming perpendicular geometry and no disk flaring). The larger distance of the first synchrotron emission region  $z_{\text{acc}}$  from the disk, combined with moderate beaming, reduces its importance for disk feedback. On the other hand, inverse Compton processes near the base of the jets can produce reflection fractions of up to  $\sim 15-20\%$ . This value is actually a lower limit because it does not include the effects of light bending, which will serve to increase the reflection fraction possibly quite significantly (Miniutti & Fabian 2004)

Beyond relaxing the assumption about the acceleration rate, there are a few other differences between this model and the synchrotron-dominated models considered in Markoff et al. (2001a) and Markoff et al. (2003). The comparatively weak inverse Compton component in prior models followed mainly from our choice of a small jet nozzle radius,  $r_0 \sim 3r_g$ , which was based on the assumption that the jet radius was on the order of the event horizon. If, on the other hand, the jet base is contiguous with, or generated in, an extended corona, a larger scale seems more sensible. With this in mind, we here consider models with typical values of  $r_0 \gtrsim 10r_g$ .

The dependence of the calculated spectrum upon the model parameters, and their interdependence, are complex. Increasing the scale of the jet base decreases the electron density as well as the magnetic field, for a fixed equipartition relationship. This allows one to consider electron temperatures several times higher than those used in our previous models (to make up for lost synchrotron flux). The higher electron temperatures lead to greater inverse Compton emission relative to synchrotron processes in the X-ray band. Alternately, one can compensate for the weakened radiating power of the decreased particle density by increasing the total power input into the jet,  $Q_j$ . Again, for a fixed equipartition relationship, the particle density is more sensitive to this change than the magnetic field (because the pressure of the field is  $\propto B^2$ ) and thus the inverse Compton component will experience a greater boost relatively.

### REFERENCES

- Arnaud, K. A. 1996, in ASP Conf. Ser. 101: Astronomical Data Analysis Software and Systems V, 17  
 Böttcher, M. & Reimer, A. 2004, ApJ, 609, 576  
 Baganoff, F. K. 2003, AAS/High Energy Astrophysics Division, 7,  
 Baganoff, F. K., Bautz, M. W., Brandt, W. N., Chartas, G., Feigelson, E. D., Garmire, G. P., Maeda, Y., Morris, M., Ricker, G. R., Townsley, L. K., & Walter, F. 2001, Nature, 413, 45  
 Baganoff, F. K., Maeda, Y., Morris, M., Bautz, M. W., Brandt, W. N., & Burrows, D. N. 2003, ApJ, 591, 891  
 Ballantyne, D. R., Iwasawa, K., & Fabian, A. C. 2001, MNRAS, 323, 506

- Belloni, T., Homan, J., Casella, P., van der Klis, M., Nespoli, E., Lewin, W. H. G., Miller, J. M., & Mendez, M. 2005, *A&A*, in press, (astro-ph/0504577)
- Beloborodov, A. M. 1999, *ApJ*, 510, L123
- Blandford, R. D. & Königl, A. 1979, *ApJ*, 232, 34
- Coppi, P. 2004, in *AIP Conf. Proc. 714: X-ray Timing 2003: Rossi and Beyond*, 79–88
- Coppi, P. S. 1999, in *ASP Conf. Ser. 161: High Energy Processes in Accreting Black Holes*, 375
- Corbel, S. & Fender, R. 2002, *ApJ*, 573, L35
- Corbel, S., Fender, R. P., Tzioumis, A. K., Nowak, M., McIntyre, V., Durouchoux, P., & Sood, R. 2000, *A&A*, 359, 251
- Corbel, S., Nowak, M., Fender, R. P., Tzioumis, A. K., & Markoff, S. 2003, *A&A*, 400, 1007
- di Matteo, T., Celotti, A., & Fabian, A. C. 1997, *MNRAS*, 291, 805
- Done, C., Mulchaey, J. S., Mushotzky, R. F., & Arnaud, K. A. 1992, *ApJ*, 395, 275
- Dove, J. B., Wilms, J., & Begelman, M. C. 1997, *ApJ*, 487, 747
- Dove, J. B., Wilms, J., Maisack, M. G., & Begelman, M. C. 1997, *ApJ*, 487, 759
- Esin, A. A., McClintock, J. E., & Narayan, R. 1997, *ApJ*, 489, 865
- Fabian, A. C., Guilbert, P. W., Motch, C., Ricketts, M., Ilovaisky, S. A., & Chevalier, C. 1982, *A&A*, 111, L9+
- Falcke, H. 1996, *ApJ*, 464, L67
- Falcke, H. & Biermann, P. L. 1995, *A&A*, 293, 665
- Falcke, H., Kording, E., & Markoff, S. 2004, *A&A*, 414, 895
- Falcke, H. & Markoff, S. 2000, *A&A*, 362, 113
- Fender, R., Corbel, S., Tzioumis, T., McIntyre, V., Campbell-Wilson, D., Nowak, M., Sood, R., Hunstead, R., Harmon, A., Durouchoux, P., & Heindl, W. 1999, *ApJ*, 519, L165
- Fender, R. P. 2001, *MNRAS*, 322, 31
- Fender, R. P. 2003, in *Compact Stellar X-ray Sources*, Eds. W.H.G. Lewin and M. van der Klis, Cambridge University Press, in press (astro-ph/0303339)
- Fender, R. P. & Kuulkers, E. 2001, *MNRAS*, 324, 923
- Gallo, E., Fender, R. P., & Pooley, G. G. 2003, *MNRAS*, 344, 60
- Gierliński, M., Zdziarski, A. A., Poutanen, J., Coppi, P. S., Ebisawa, K., & Johnson, W. N. 1999, *MNRAS*, 309, 496
- Gleißner, T., Wilms, J., Pooley, G. G., Nowak, M. A., Pottschmidt, K., Markoff, S., Heinz, S., Klein-Wolt, M., Fender, R. P., & Staubert, R. 2004a, *A&A*, 425, 1061
- Gleißner, T., Wilms, J., Pottschmidt, K., Uttley, P., Nowak, M. A., & Staubert, R. 2004b, *A&A*, 414, 1091
- Hannikainen, D. C., Hunstead, R. W., Campbell-Wilson, D., & Sood, R. K. 1998, *A&A*, 337, 460
- Hawley, J. F. & Krolik, J. H. 2001, *ApJ*, 548, 348
- Heinz, S. & Sunyaev, R. A. 2003, *MNRAS*, 343, L59
- Ho, L. C. 1999, *ApJ*, 516, 672
- Homan, J. & Belloni, T. 2005, in *From X-ray Binaries to Quasars: Black Hole Accretion on All Mass Scales*, ed. T. J. Maccarone, R. P. Fender, L. C. Ho (Dordrecht: Kluwer), in press, (astro-ph/0412597)
- Homan, J., Buxton, M., Markoff, S., Bailyn, C. D., Nespoli, E., & Belloni, T. 2005, *ApJ*, 624, 295
- Houck, J. C. & Denicola, L. A. 2000, in *ASP Conf. Ser. 216: Astronomical Data Analysis Software and Systems IX*, Vol. 9, 591
- Hynes, R. I., Steeghs, D., Casares, J., Charles, P. A., & O'Brien, K. 2003, *ApJ*, 583, L95
- , 2004, *ApJ*, 609, 317
- Ibragimov, A., Poutanen, J., Gilfanov, M., Zdziarski, A. A., & Shrader, C. R. 2005, *MNRAS*, submitted (astro-ph/0502423)
- Jahoda, K., Swank, J. H., Giles, A. B., Stark, M. J., Strohmayer, T., Zhang, W., & Morgan, E. H. 1996, in *Proc. SPIE Vol. 2808*, p. 59-70, EUV, X-Ray, and Gamma-Ray Instrumentation for Astronomy VII, Oswald H. Siegmund; Mark A. Gummin; Eds., 59–70
- Jester, S., Röser, H.-J., Meisenheimer, K., Perley, R., & Conway, R. 2001, *A&A*, 373, 447
- Jokipii, J. R. 1987, *ApJ*, 313, 842
- Levine, A. M., Bradt, H., Cui, W., Jernigan, J. G., Morgan, E. H., Remillard, R., Shirey, R. E., & Smith, D. A. 1996, *ApJ*, 469, L33+
- Lightman, A. P. & White, T. R. 1988, *ApJ*, 335, 57
- Maccarone, T. J. 2003, *A&A*, 409, 697
- Magdziarz, P. & Zdziarski, A. A. 1995, *MNRAS*, 273, 837
- Makishima, K., Maejima, Y., Mitsuda, K., Bradt, H. V., Remillard, R. A., Tuohy, I. R., Hoshi, R., & Nakagawa, M. 1986, *ApJ*, 308, 635
- Malzac, J., Beloborodov, A. M., & Poutanen, J. 2001, *MNRAS*, 326, 417
- Mannheim, K. 1993, *A&A*, 269, 67
- Markoff, S. 2005, *ApJ*, 618, L103
- Markoff, S., Falcke, H., & Fender, R. 2001a, *A&A*, 372, L25
- Markoff, S., Falcke, H., Yuan, F., & Biermann, P. L. 2001b, *A&A*, 379, L13
- Markoff, S., Melia, F., & Sarcevic, I. 1999, *ApJ*, 522, 870
- Markoff, S., Nowak, M., Corbel, S., Fender, R., & Falcke, H. 2003, *A&A*, 397, 645
- Markoff, S. & Nowak, M. A. 2004, *ApJ*, 609, 972
- Marscher, A. P. & Gear, W. K. 1985, *ApJ*, 298, 114
- McClintock, J. E. & Remillard, R. A. 2003, in *Compact Stellar X-ray Sources*, Eds. W.H.G. Lewin and M. van der Klis, Cambridge University Press, in press (astro-ph/0306213)
- Meier, D. L. & Nakamura, M. 2004, in *Proceedings of the "3-D signatures in Stellar Explosions" Workshop*, 10-13 June, 2003, , in press
- Melia, F. & Falcke, H. 2001, *ARA&A*, 39, 309
- Merloni, A., Di Matteo, T., & Fabian, A. C. 2000, *MNRAS*, 318, L15
- Merloni, A., Heinz, S., & di Matteo, T. 2003, *MNRAS*, 345, 1057
- Miller, J. A. 1998, *Space Science Reviews*, 86, 79
- Miller, J. M., Ballantyne, D. R., Fabian, A. C., & Lewin, W. H. G. 2002, *MNRAS*, 335, 865
- Miller, J. M., Raymond, J., Fabian, A. C., Homan, J., Nowak, M. A., Wijnands, R., van der Klis, M., Belloni, T., Tomsick, J. A., Smith, D. M., Charles, P. A., & Lewin, W. H. G. 2004, *ApJ*, 601, 450
- Miller, K. A. & Stone, J. M. 2000, *ApJ*, 534, 398
- Miniutti, G. & Fabian, A. C. 2004, *MNRAS*, 349, 1435
- Mitsuda, K., Inoue, H., Koyama, K., Makishima, K., Matsuoka, M., Ogawara, Y., Shibasaki, N., Suzuki, K., Yanaka, Y., & Hirano, Y. 1984, *PASJ*, 36, 741
- Motch, C., Ilovaisky, S. A., & Chevalier, C. 1982, *A&A*, 109, L1
- Narayan, R., Mahadevan, R., Grindlay, J. E., Popham, R. G., & Gammie, C. 1998, *ApJ*, 492, 554
- Nayakshin, S. 2000, *ApJ*, 534, 718
- Nowak, M. A., Vaughan, B. A., Wilms, J., Dove, J. B., & Begelman, M. C. 1999, *ApJ*, 510, 874
- Nowak, M. A., Wilms, J., & Dove, J. B. 2002, *MNRAS*, 332, 856
- Nowak, M. A., Wilms, J., Heinz, S., Pooley, G., & Corbel, S. 2005, *ApJ*, submitted
- Paczynski, B. & Wiita, P. J. 1980, *Å*, 88, 23
- Pottschmidt, K., Wilms, J., Nowak, M. A., Pooley, G. G., Gleißner, T., Heindl, W. A., Smith, D. M., Remillard, R., & Staubert, R. 2003, *A&A*, 407, 1039
- Poutanen, J. 1998, in *Theory of Black Hole Accretion Disks*, Cambridge University Press, 100
- Quataert, E. & Gruzinov, A. 1999, *ApJ*, 520, 248
- Ross, R. R. & Fabian, A. C. 1993, *MNRAS*, 261, 74
- , 2005, *MNRAS*, 358, 211
- Ross, R. R., Fabian, A. C., & Young, A. 1999, *MNRAS*, 306, 462
- Rothschild, R. E., Blanco, P. R., Gruber, D. E., Heindl, W. A., MacDonald, D. R., Marsden, D. C., Pelling, M. R., Wayne, L. R., & Hink, P. L. 1998, *ApJ*, 496, 538
- Stern, B. E., Poutanen, J., Svensson, R., Sikora, M., & Begelman, M. C. 1995, *ApJ*, L13
- Wardziński, G. & Zdziarski, A. A. 2000, *MNRAS*, 314, 183
- Wilms, J., Nowak, M. A., Dove, J. B., Fender, R. P., & di Matteo, T. 1999, *ApJ*, 522, 460
- Wilms, J., Nowak, M. A., Pottschmidt, K., Pooley, G., & Fritz, S. 2005, *A&A*, submitted
- Wu, K., Soria, R., Hunstead, R. W., & Johnston, H. M. 2001, *MNRAS*, 320, 177
- Young, A. J. & Reynolds, C. S. 2000, *ApJ*, 529, 101
- Zdziarski, A. A., Gierliński, M., Mikołajewska, J., Wardziński, G., Smith, D. M., Alan Harmon, B., & Kitamoto, S. 2004, *MNRAS*, 351, 791

TABLE A2. GX 339–4 AND CYG X-1 JET MODEL FITS (90% CONFIDENCE LEVEL ERROR BARS)

Obs ID	$N_j$ ( $10^{-3} L_{\text{Edd}}$ )	$^a L_j$ ( $10^{-3} L_{\text{Edd}}$ )	$r_0$ ( $GM/c^2$ )	$T_e$ ( $10^{10}$ K)	$p$	$k$	$pl_f$	$z_{\text{acc}}$	$h_0$
20181-01-02	$1.27^{+0.03}_{-0.02}$	7.9	$20.2^{+0.3}_{-0.3}$	$5.01^{+0.07}_{-0.08}$	$2.94^{+0.01}_{-0.02}$	$1.75^{+0.09}_{-0.09}$	$0.67^{+0.03}_{-0.02}$	25	$1.34^{+0.02}_{-0.02}$
40108-02-01	$0.64^{+0.02}_{-0.03}$	4.7	$9.6^{+0.5}_{-0.1}$	$5.23^{+0.13}_{-0.12}$	$2.39^{+0.01}_{-0.00}$	$1.12^{+0.01}_{-0.01}$	$0.74^{+0.05}_{-0.01}$	302	$1.41^{+0.01}_{-0.01}$
40108-02-03	$0.34^{+0.01}_{-0.03}$	2.1	$10.9^{+0.8}_{-3.2}$	4.0	$2.65^{+0.01}_{-0.00}$	2.2	0.7	87	$1.29^{+0.03}_{-0.14}$
40099-01-19	$0.85^{+0.02}_{-0.03}$	7.4	$9.1^{+0.2}_{-0.2}$	$3.62^{+0.05}_{-0.04}$	$2.50^{+0.03}_{-0.02}$	$1.99^{+0.18}_{-0.11}$	$0.76^{+0.02}_{-0.04}$	16	$1.33^{+0.02}_{-0.02}$
60090-01-26	$0.74^{+0.01}_{-0.01}$	7.1	$4.4^{+0.2}_{-0.1}$	$3.28^{+0.01}_{-0.01}$	$2.61^{+0.01}_{-0.01}$	$1.77^{+0.04}_{-0.01}$	$0.73^{+0.08}_{-0.02}$	9	$1.18^{+0.00}_{-0.00}$
60090-01-41	$0.78^{+0.02}_{-0.04}$	6.4	$6.7^{+0.1}_{-0.3}$	$3.90^{+0.03}_{-0.02}$	$2.65^{+0.01}_{-0.01}$	$1.70^{+0.01}_{-0.13}$	$0.81^{+0.03}_{-0.01}$	14	$1.17^{+0.05}_{-0.00}$

NOTE. — We failed to resolve 90% confidence level error bars for parameters listed in italics. Jet model parameters are described in the paper and Appendix. Upper half of the table refers to GX 339–4, while the lower half refers to Cyg X-1. We fixed the mass, distance and inclination of GX 339–4 and Cyg X-1 to 7 and 10  $M_{\odot}$ , 6 and 2.5 kpc, and 30° and 47°, respectively (Hynes et al. 2003, 2004; Wu et al. 2001; Nowak et al. 1999). <sup>a</sup>Total output power from the jets in their rest frames  $L_j$  is listed for completeness but is not itself a fitted parameter (see discussion in the Appendix).

TABLE A3. GX 339–4 AND CYG X-1 JET MODEL FITS, CONTINUED

Obs ID	$u_{\text{acc}}/c$	$f_{\text{sc}}$	$L_{\text{disk}}$ ( $10^{-3} L_{\text{Edd}}$ )	$T_{\text{disk}}$ (keV)	$^b r_{\text{in}}$ ( $r_g$ )	$A_{\text{line}}$ ( $10^{-2}$ )	$E_{\text{line}}$ (keV)	$\sigma$ (keV)	$\Omega/2\pi$	$\chi^2/\text{DoF}$
20181-01-02	$0.79^{+0.06}_{-0.09}$	$1000^{+70}_{-210}$	$99^{+1}_{-2}$	$0.06^{+0.16}_{-0.05}$	486	$0.30^{+0.04}_{-0.03}$	$6.3^{+0.1}_{-0.1}$	$1.0^{+0.1}_{-0.1}$	$0.14^{+0.01}_{-0.03}$	179/109
40108-02-01	$0.32^{+0.05}_{-0.00}$	$1100^{+200}_{-800}$	$0.33^{+0.01}_{-0.01}$	$1.53^{+0.12}_{-0.10}$	0.04	$0.09^{+0.03}_{-0.03}$	$6.4^{+0.1}_{-0.1}$	$0.7^{+0.2}_{-0.2}$	$0.00^{+0.06}_{-0.00}$	118/87
40108-02-03	0.57	230	0.1	0.36	0.4	$0.012^{+0.006}_{-0.002}$	$6.4^{+0.2}_{-0.2}$	$0.6^{+0.2}_{-0.2}$	$0.21^{+0.11}_{-0.21}$	22/36
40099-01-19	$0.55^{+0.07}_{-0.01}$	$940^{+50}_{-200}$	$2.4^{+0.8}_{-0.6}$	$0.71^{+0.07}_{-0.06}$	0.5	$4.5^{+0.4}_{-0.7}$	$6.1^{+0.2}_{-0.1}$	$1.1^{+0.1}_{-0.1}$	$0.19^{+0.02}_{-0.01}$	225/154
60090-01-26	$0.35^{+0.00}_{-0.00}$	$790^{+10}_{-10}$	$0.8^{+0.1}_{-0.1}$	$0.98^{+0.11}_{-0.09}$	0.1	$2.3^{+0.2}_{-0.5}$	$6.0^{+0.1}_{-0.0}$	$0.9^{+0.1}_{-0.1}$	$0.00^{+0.01}_{-0.00}$	207/177
60090-01-41	$0.38^{+0.05}_{-0.01}$	$710^{+10}_{-170}$	$0.8^{+0.2}_{-0.4}$	$0.88^{+0.10}_{-0.03}$	0.2	$1.8^{+0.3}_{-0.1}$	$6.1^{+0.2}_{-0.1}$	$0.9^{+0.2}_{-0.1}$	$0.02^{+0.11}_{-0.02}$	186/179

NOTE. — We failed to resolve 90% confidence level error bars for parameters listed in italics. Jet model parameters are described in the paper and Appendices. Line parameters correspond to the usual XSPEC/ISIS normalization, centroid energy, and width of the `gauss` line model.  $\Omega/2\pi$  is the reflection fraction from the XSPEC/ISIS `reflect` model. Upper half of the table refers to GX 339–4, while the lower half refers to Cyg X-1. <sup>b</sup>Values listed for inner disk radius  $r_{\text{in}}$  are derived from the spectrally difficult-to-constrain fitted parameters  $L_{\text{disk}}$  and  $T_{\text{disk}}$ , and are thus also unconstrained: see discussion in Section 4.

TABLE A4. GX 339–4 AND CYG X-1 CORONAL MODEL FITS (90% CONFIDENCE LEVEL ERROR BARS)

Obs ID	$A_{\text{eqpair}}$ ( $10^{-3}$ )	$\ell_{\text{h}}/\ell_{\text{s}}$	$\tau_p$	$A_{\text{disk}}$ ( $10^{-5}$ )	$T_{\text{disk}}$ (keV)	$A_{\text{line}}$ ( $10^{-2}$ )	$E_{\text{line}}$ (keV)	$\sigma$ (keV)	$\Omega/2\pi$	$\xi$ ( $4\pi F/n$ )	$\chi^2/\text{DoF}$
20181-01-02	$0.21^{+0.00}_{-0.07}$	$5.85^{+0.48}_{-0.33}$	$2.86^{+0.25}_{-0.08}$	$4.0^{+1.4}_{-0.8}$	$1.30^{+0.16}_{-0.24}$	$0.14^{+0.10}_{-0.04}$	$6.4^{+0.1}_{-0.1}$	$0.5^{+0.4}_{-0.2}$	$0.11^{+0.03}_{-0.04}$	$680^{+1460}_{-520}$	170/111
40108-02-01	$0.11^{+0.03}_{-0.02}$	$7.38^{+0.55}_{-0.51}$	$1.79^{+0.65}_{-0.59}$	$1.1^{+1.3}_{-0.8}$	$1.35^{+0.16}_{-0.21}$	$0.06^{+0.04}_{-0.02}$	$6.4^{+0.1}_{-0.1}$	$0.4^{+0.3}_{-0.4}$	$0.10^{+0.04}_{-0.05}$	$560^{+3790}_{-560}$	117/90
40108-02-03	$0.03^{+0.00}_{-0.09}$	$3.73^{+1.12}_{-0.28}$	$6.69^{+0.92}_{-2.87}$	$1.0^{+0.8}_{-0.6}$	$1.10^{+0.30}_{-0.31}$	$0.02^{+0.01}_{-0.01}$	$6.4^{+0.2}_{-0.2}$	$0.7^{+0.3}_{-0.4}$	$0.00^{+0.26}_{-0.00}$	...	17/37
40099-01-19	$9.23^{+0.01}_{-0.01}$	$3.60^{+0.01}_{-0.01}$	$1.35^{+0.01}_{-0.01}$	$422^{+12}_{-3}$	$0.85^{+0.01}_{-0.01}$	$2.5^{+0.1}_{-0.1}$	$6.2^{+0.1}_{-0.0}$	$0.8^{+0.0}_{-0.1}$	$0.19^{+0.01}_{-0.01}$	$1140^{+100}_{-170}$	226/158
60090-01-26	$6.78^{+0.14}_{-2.11}$	$5.88^{+0.06}_{-0.07}$	$1.64^{+0.02}_{-0.02}$	$47^{+12}_{-8}$	$0.87^{+0.13}_{-0.00}$	$1.9^{+0.1}_{-0.2}$	$6.0^{+0.1}_{-0.0}$	$0.9^{+0.0}_{-0.1}$	$0.22^{+0.01}_{-0.01}$	$2^{+13}_{-2}$	191/181
60090-01-41	$6.09^{+1.57}_{-1.19}$	$5.67^{+0.11}_{-0.05}$	$1.49^{+0.02}_{-0.06}$	$49^{+13}_{-11}$	$0.85^{+0.15}_{-0.04}$	$1.4^{+0.1}_{-0.2}$	$6.2^{+0.0}_{-0.1}$	$0.8^{+0.1}_{-0.1}$	$0.22^{+0.01}_{-0.01}$	$2^{+15}_{-2}$	186/183

NOTE. — Model parameters are for the XSPEC/ISIS implementations of the `eqpair` model with ionized, smeared reflection, with additional contributions from a `diskpn` and `gauss` model. Upper half of the table refers to GX 339–4, while the lower half refers to Cyg X-1.